ORIGINAL ARTICLE

Spherical edge burr formation during servo valve spool shoulder grinding: identifying the formation mechanism and designing a deburring device

Yuefeng Li[1] · Min Wang[1] · Zhongyu An[1]

Abstract

The basis for the formation of spherical edge burrs during servo valve spool shoulder grinding and a method for eliminating these burrs were investigated. Based on the results of this investigation, a grinding and synchronous deburring device was designed. A geometric model of single abrasive grains was established and the formation mechanism of the valve spool edge burrs was evaluated. Subsequently, the deburring process was analyzed via dynamic simulations, and based on the results, the aforementioned device was designed for mounting on an S20 precision cylindrical grinder. The correctness of the simulation and the feasibility of the device were verified via experiments. The experimentally observed burr shape and size corresponded closely to the simulated features. Moreover, the test device was effective in removing the edge burrs of the valve spool, as evidenced by the lack of sharp edge burrs. Hence, this device could be helpful in grinding the valve spool shoulder for significant improvement in the processing quality and efficiency.

Keywords Valve spool grinding · Single abrasive grain · Spherical edge burr · Deburring

1 Introduction

Due to its rapid response, high output power, and high measurement and precision control, an electro-hydraulic servo system plays an important role in intelligent manufacturing. The main component of these systems, i.e., an electro-hydraulic servo valve, is responsible for electro-hydraulic energy conversion and power amplification [1–3]. The slide valve deputy (Fig. 1) is a key component of the valve, which consists of a valve spool and a valve sleeve. The relative motion of the two components can change the amount of overlap, thereby achieving control of the liquid flow. To ensure the accuracy of the overlap and overflow, a sharp edge of the valve spool (without burrs) should be maintained (overlap precision required—on the order of microns). In general, edges with a rounded radius of $R < 0.005$ mm are referred to as retained sharp edges [4]. Axis parts are typically easier to process than hole parts, and hence, the grinding process of the

slide valve deputy is generally based on the valve sleeve to grind the valve spool. Therefore, the manufacturing precision of a valve spool shoulder and the related dimensional tolerance requirements are very high, and will directly affect the performance of an electro-hydraulic servo valve system. A study focused on improving the manufacturing precision of the valve spool shoulder is therefore warranted.

The processing of the valve spool shoulder is typically performed on an S20 precision cylindrical grinder, capable of both rough grinding and fine grinding. During the grinding process, burrs are formed on the edge of the shoulder. These burrs may reduce the processing efficiency and surface quality, and hence, must be removed or avoided. In the past, burrs were usually removed via manual grinding, but the manual deburring process leads to poor processing quality and low efficiency [5]. Xu et al. proposed a magnetic grinding method for removing burrs from the edges of precision parts, that is, by placing different types of abrasives between the workpiece and the magnetic pole. The abrasives generate positive pressure to the workpiece end under the action of a magnetic force. The magnetic pole drives rotation of the workpiece, resulting in interaction between the abrasives and the workpiece, and in turn, burr removal [6]. However, this method is relatively inefficient, the operation is cumbersome, and the rejection rate is high. Guo et al. proposed a thermal deburring method where

✉ Yuefeng Li
yuefengli@hit.edu.cn

1 School of Mechatronics Engineering, Harbin Institute of Technology, Harbin 150001, Heilongjiang, China

Fig. 1 Spool valve substructure diagram
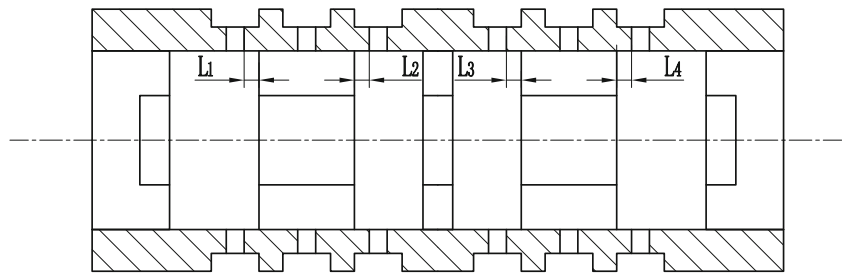
a part is placed in a fully sealed appliance. A high-pressure gas is then detonated in the appliance, thereby generating a high-energy impact force for removing burrs from the edges of the part. However, this method is very complex and setup of the application equipment system is difficult [7]. Li proposed a discharge machining deburring method, where burrs are removed using a discharge between the electrodes. Control of the distance is, however, difficult. Therefore, to minimize the occurrence of burrs, studies have focused on determining the burr formation mechanism and predicting the processing results, with the aim of identifying the ideal grinding conditions.

Nowadays, the following general steps are performed during the removal of edge burrs from the precision rotary parts that maintain sharp edges: (1) the workpiece is placed on the chuck of the special machine tool, (2) the spindle is fixed into place and then rotated, (3) sharp edge burrs are removed with oil stone, and (4) sandpaper is used to polish radially and axially along the edges, and a nylon brush or polishing wheel is used for polishing [8–10]. Although this method improves the yield, drawbacks such as low efficiency, high labor intensity, high requirements for technicians, and inability to mass produce the valve spool have proven elusive. High production efficiency and accuracy of the valve spool and, consequently, automation of the valve spool production require improvement in the processing technology.

Therefore, a method suitable for shoulder edge burr prediction and online deburring is presented in the present paper. A geometric model of single abrasive grains is established, and the formation mechanism of valve spool edge burrs is evaluated. After the burr shape and size are obtained, a dynamic simulation of the deburring is performed in order to determine the optimal removal parameters. Based on the deburring simulation results and the existing spool shoulder processing technology, an auxiliary device for online deburring is designed. The feasibility and effectiveness of this device are assessed through processing experiment and measurements.

2 Analysis of edge burr formation and removal

The grinding method of the spool shoulder is face grinding, i.e., both sides of the grinding wheel stick against the end surface of the shoulder for grinding, where the essence is the micro-cutting process, many irregularly shaped abrasive grains are discretely distributed on the surface of the grinding wheel. As shown in Fig. 2, the movement during the grinding process can be divided into three regimes. These correspond to the high-speed rotation motion of the grinding wheel along its axis, rotation motion of the workpiece (the valve spool), and linear motion of the workpiece along its axis, which represent the grinding linear velocity, feed movement, and grinding depth, respectively, in three cutting elements.

2.1 Mechanical analysis of burr formation

The burr of the spool shoulder is generated on the edge, resulting from the coupling of the cutting-in and cutting-out effect of the abrasive grains. For grinding, the burrs produced in the cutting-out direction are considerably larger than those generated in the cutting-in direction, and hence, the cutting-in effect can be ignored [11–13]. Furthermore, the linear velocity of the grinding wheel is significantly larger than the rotational velocity of the valve spool. The formation process of burrs can therefore be simplified to the linear cutting movement of the abrasive grain, as shown in Fig. 3.

Immediately preceding the cutting out of the abrasive grain, this grain will have an extrusion effect on the edge. The cutting action of the grain on the edge material plays a key in the formation of the burr [12]. Figure 4 shows the cutting model of the abrasive grain during cutting.

As shown in Fig. 4, F_c is the force applied on the cutting layer in the cutting-out direction. F_a and F_b are two
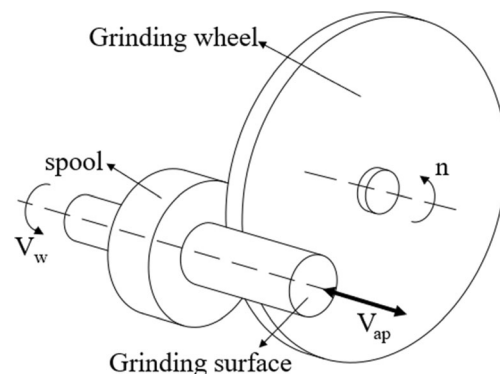
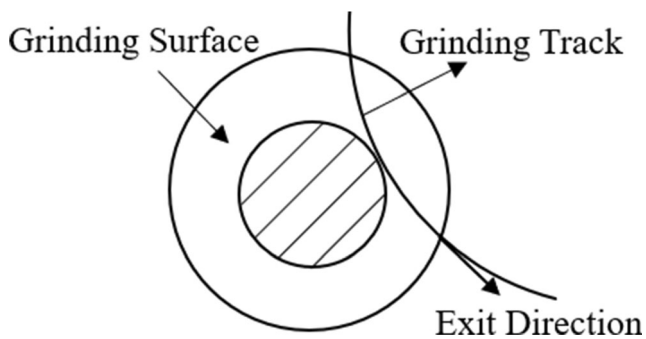

Fig. 2 Spool shoulder machining diagram

Fig. 3 Schematic showing shoulder burr formation

component forces of F_c, which induce plastic bending deformation and shear-slip deformation in the cross-section, respectively. For the cutting process, the force exerted on the top of the tool is the largest and gradually decreases along the tool edge. Therefore, the assumption is that the force of the tool on the workpiece could be described by a triangular distribution, and the corresponding mechanical model is

$$\sigma_x = \sigma_m(l-x)/l \tag{1}$$

where σ_x is the stress applied by the tool at a distance x from the cutting layer of the workpiece, σ_m is the average stress, l is the contact length, a_p is the cutting depth, and κ_r is the main declination. The cutting resultant force is obtained by integrating the previous equation:

$$F_{xy} = \delta_w \int_0^l \frac{l-x}{l} dx = \frac{l}{2}\delta_w\sigma_m \tag{2}$$

where F_{xy} is the cutting resultant force and δ_w is the magnitude of change in the cutting layer.

When the tool moves forward by Δx, the work done by the bending component force F_a is

$$W_a = F_a\Delta x cos\varphi = F_c\Delta x cos2\varphi \tag{3}$$

The work done by the shear slip component force F_b is

$$W_b = F_b\Delta x sin\varphi = F_c\Delta x sin\varphi \tag{4}$$

After the abrasive grain cutting, the swarfs and burrs form a coupling effect. Edge burrs are generally classified as primary
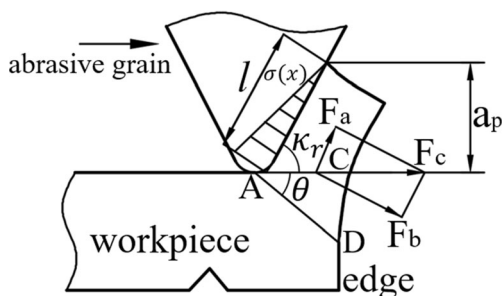
burrs and secondary burrs. For $W_a > W_b$ during the cutting process, the edge deformation is dominated by bending deformation, resulting in primary burrs with an uneven size distribution and a relatively large amount of bending. The edge deformation is dominated by shear slip deformation when $W_a < W_b$, resulting in secondary burrs characterized by a uniform size distribution and easy removal.

2.2 Geometric model of single abrasive grain

The micro-cutting motion of a single abrasive grain occurs during the grinding process of the spool shoulder. Therefore, the simulation process can be simplified to the single-grain micro-cutting process. Through the simulation analysis of a single abrasive grain, theoretical support is provided for studying the formation mechanism of edge burrs. The shape of the abrasive grain distributed on the grinding wheel is relatively complex. In studies of grinding processes, this shape is usually simplified to a conical shape with a spherical top [14–16]. The main geometric parameters are the top diameter d, taper angle θ, and radius of the sphere r (the shape is shown in Fig. 5). The geometric relationship between the parameters is given as follows:

$$r = \frac{1}{16}d + 1.75 \tag{5}$$

$$\theta = \frac{1}{35}r + 98 \tag{6}$$

The empirical conversion formula for the number of meshes and the particle size is

$$M = 14832.4/n \tag{7}$$

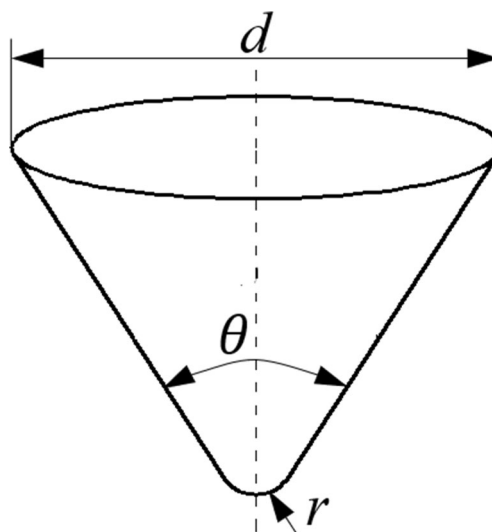Fig. 4 Edge cutting direction burr formation model

Fig. 5 Single abrasive grain geometry

where M represents the particle size and n represents the mesh number. The grinding wheel material for the spool shoulder grinding process is 128 mesh of green corundum. According to this formula, the top diameter of the abrasive grain, radius of the sphere, and the cone angle are 116 μm, 9 μm, and 49.13°, respectively.

The valve spool is fabricated from 440c, which is a high carbon and high chromium tool steel with good hardenability, high hardness, and good wear resistance at medium temperatures.

In the grinding process of the valve spool, the main processing parameters are the line speed of the grinding wheel (25–40 m/s) and the axial movement speed of the valve spool (1–5 μm/s). Simulations of single abrasive grain micro-cutting were performed using these parameters. In addition to setting the geometric motion parameters of the cutting process, for close correspondence between the simulation model and the actual effect, the separation criterion, damage failure model, and friction model are selected. In this work, a separation criterion based on the equivalent plastic strain is used to reflect the nature of material fracture deformation. The value of the measure reflecting the fracture parameter is determined as follows:

$$W = \Sigma \left(\frac{\Delta \overline{\varepsilon}^{pl}}{\overline{\varepsilon}_f^{pl}} \right) \tag{8}$$

where $\overline{\varepsilon}^{pl}$ is the strain at material fracture failure and $\Delta \overline{\varepsilon}^{pl}$ is the increment of equivalent plastic strain in each load increment step. The incremental steps of the entire cutting process are cumulatively superimposed. When the value of w accumulates to 1, the fracture failure of the material is determined.

The flexible damage model [17] is selected as the damage failure model of the material. The model assumes that the equivalent plastic strain at the time of damage initiation is a function of the triaxial stress and strain rate. The relevant parameters are the fracture strain, stress triaxiality, and strain rate. In addition, the damage evolution model uses displacement to determine the damage variable. The setting of the damage displacement value is based on the fracture strain and the mesh size of the material, which is equal to the fracture strain multiplied by the characteristic size of an element. This parameter plays a key role in the fracture and formation of swarfs.

During the cutting process, a slip zone and a bonding zone are generated in the contact area between the abrasive grain and the workpiece. The frictional force of the blade contact area can be defined as follows:

$$\tau_f(x) = k_{swarf}, \mu\sigma_n(x) \geq k_{swarf} \left(0 \leq x \leq l_p \right) \tag{9}$$

$$\tau_f(x) = \mu\sigma_n, \mu\sigma_n, (x) \leq k_{swarf} \left(l_p \leq x \leq l_c \right) \tag{10}$$

where $\tau_f(x)$ is the friction shear stress, k_{swarf} is the critical shear flow stress, σ_n is the normal stress, and μ is the friction coefficient.

A geometric model that incorporates material parameters, motion parameters, a damage model, and a contact friction model of single abrasive grain micro-cutting was established. Afterward, ABAQUS was used to simulate the cutting process in order to determine the formation principle of edge burrs.

2.3 Simulation analysis of burr formation

Based on the simulation results of ABAQUS, the cutting process can be divided into five phases: initial cutting, continuous cutting, edge rotation deformation, burr development, and final forming. The last three phases are directly related to edge burr formation, and the study of these phases will be helpful in determining the principle of this formation.

During the entire cutting process, as the abrasive grain continues to advance, the distance between the grain and the edges decreases, and the elastic deformation regions continue to expand toward the edge. The edge rotation deformation phase is shown in Fig. 6. In the initial phase, the edge support stiffness decreases gradually as the abrasive grain approaches, under the action of the cutting force. Consequently, the edge begins to elastically deform around point D. This point is referred to as the fulcrum, and the distance between the
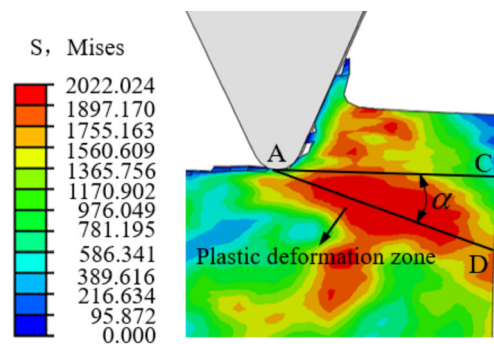
(a) Initial phase of rotational deformation
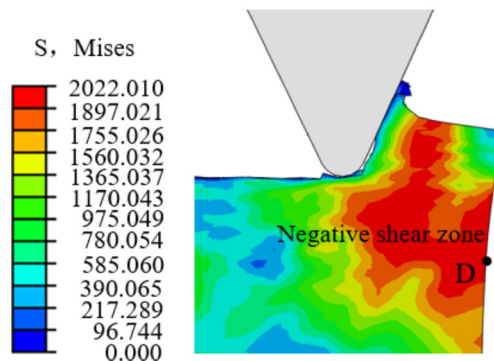
(b) Rotational deformation phase

Fig. 6 Edge rotation deformation phase. (a) Initial phase of rotational deformation. (b) Rotational deformation phase

fulcrum and the machined plane determines the thickness of the burr. In this phase, the region near the edge produces a negative deformation angle α, i.e., the angle between AC and AD, where the deformation direction of the material lies below the edge. Under the action of the cutting force, the stress of the workpiece edge increases gradually, eventually exceeding the yield limit of the material, and the deformation changes from elastic deformation to plastic deformation [18]. The edge also undergoes plastic deformation around point D (see Fig. 6). A high stress zone is generated at the fulcrum (D), and the maximum stress is 2022 MPa. In this phase, the internal material of the workpiece gives rise to a shear slip zone (i.e., a negative shear zone) along the machined face. As the abrasive grain advances, the negative shear zone gradually expands toward the edge. The direction of the stress gradient in this area will directly determine the final shape and size of the burr, which is key to the formation of the burr. The generation and expansion of the negative shear zone represent the most significant features of this phase.

When the rotational deformation phase begins, the workpiece edge undergoes increasingly severe deformation. Figure 7 shows the development phase of the burr. In this phase, the stress value of the edge region decreases, and the plastic deformation is restored to the elastic deformation level, but the deformation value of the plastic segment is retained. The contact area between the abrasive grain and the workpiece is gradually reduced, and the corresponding pressing decreases. Similarly, the stress at the joint of the workpiece end and the swarfs decreases continuously. The edge curvature gradually exceeds the critical value, resulting eventually in the shedding of swarfs and the formation of burrs. In this phase, the root area of the cutting layer will generate a bending moment around point D under the cutting action of the abrasive grain. The bending magnitude of the material around the edge of the workpiece increases continuously and deviates gradually from the movement path of the abrasive grain along the cutting direction. Upon reaching a certain point, the workpiece will be completely detached from the front cutting edge of the abrasive grain. Subsequently, the abrasive grain
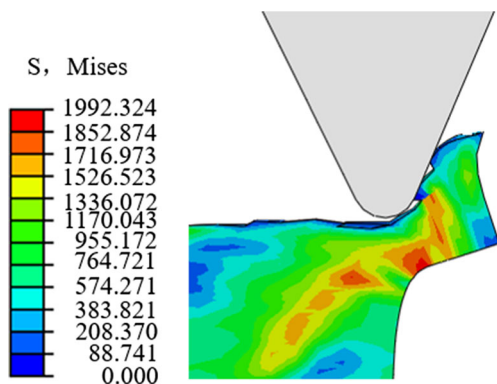

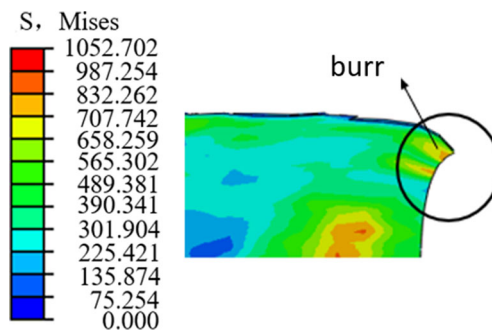**Fig. 7** Burr development phase

**Fig. 8** Final forming phase

becomes separated from the workpiece and involvement of this grain in workpiece cutting ceases. The bending deformation of the edge root material represents a distinct feature of the rotational deformation phase.

Figure 8 shows the final forming phase of the burr. In this process, when the bending stress of the cut edge (rotational deformation region) exceeds its critical value, the edge falls off and forms swarfs. The stress value in the residual area of the workpiece edge decreases sharply, and the deformation is gradually restored. However, due to the large prior plastic deformation, complete restoration of the original shape is impossible; there is still some residual deformation. The element deformation around the edge accumulates and interacts, eventually resulting in the formation of burrs. At the end of burr formation, a small amount of residual stress persists on the workpiece edge, and this stress must be eliminated.

Simulations of burr formation revealed that the formation of edge burrs is induced mainly by the plastic yield flow generated by the root material in the cutting layer along the negative shear direction. In the process of abrasive cutting, the material deforms at the workpiece edge, flows and accumulates gradually, and produces burrs under the superposition effect of deformation. The formation of a negative shear zone and, consequently, the formation of burrs are affected by several factors including the cutting depth and the shear angle between the abrasive grain and the workpiece. The results of this simulation suggested that plastic bending deformation plays the key role in burr formation, and secondary burrs with relatively uniform size are formed.

## 2.4 Simulation analysis of burr removal

The burr-edge size of the spool shoulder has a direct effect on the accuracy of the spool stack, and hence, burrs must be removed during subsequent processing. Burr removal can be performed via many methods, such as turning and grinding, which occur during the micro-cutting removal process of materials [19, 20]. In this work, the ABAQUS software was used to perform dynamic simulations of burr removal and to determine the cutting force values. Figure 9 shows the burr simulation model and the final removal effect. In this simulation,

(a) Simulation model
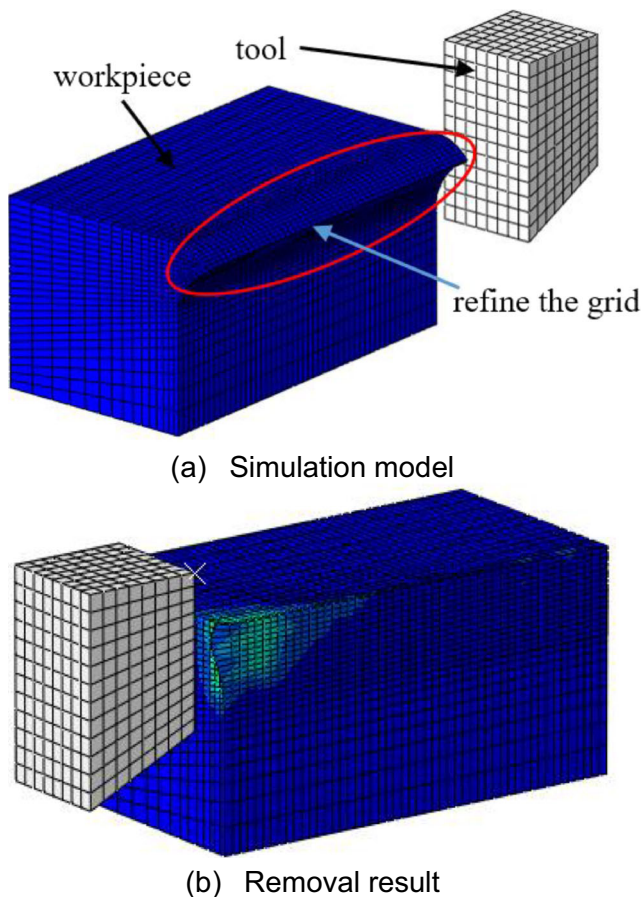
(b) Removal result

Fig. 9 Burr removal dynamic simulation. (**a**) Simulation model. (**b**) Removal result

the tool is set to a rigid body and follows reference point motion.

The reaction force of the tool reference point is the feedback force for cutting the burr (see Fig. 10 for the corresponding time-dependence of the force). As shown in the figure, the cutting force increases to ~ 1 N in ~0.13 s and remains at this value for ~0.32 s. The deburring device can be designed based
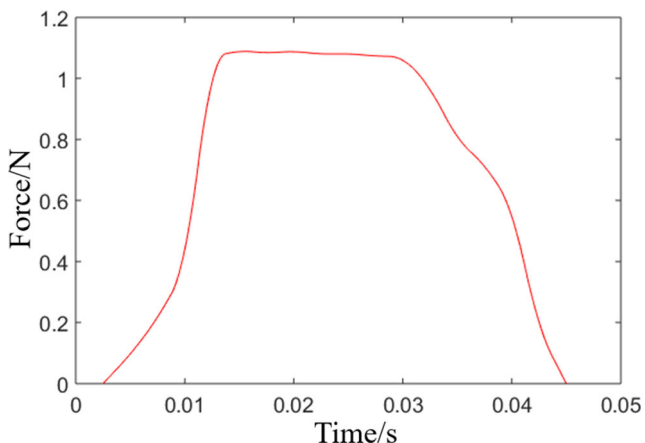
Fig. 10 Time-dependent changes in the cutting force

on the deburring cutting force determined from the simulation results.

3 Design of test device

The processing of the valve spool shoulder is generally performed by grinding with a S20 precision cylindrical grinder, and then completed by manual grinding, leading to a relatively low efficiency. To improve the processing efficiency, in this work, an online deburring device combined with an S20 grinder is designed to achieve online real-time deburring and improvements in the processing precision and efficiency of the valve spool.

3.1 Overall scheme design of the device

To meet the processing requirements, the entire device is composed of four modules: micro-drive platform, grinding detection process, deburring process, and control box [21], which can be directly mounted on the S20 precision cylindrical grinder and can be installed on demand. Among them, the micro-drive platform realizes the automatic control of the micro-feed connected to the axial dimension of the grinding device through the detachable external servo motor structure. This module is connected to the micro-feed handwheel through screws (thereby preventing damage to the original part of the machine), is easily assembled and disassembled, and can meet the axial driving requirements of the valve spool.

The device must be suspended on the S20 grinder. An extremely small and lightweight device is desired. Therefore, the grinding detection module is integrated with the deburring module. The movement along the spool axial direction can occur on a common a platform. Due to the different distance and method of radial movement, however, a separate platform is needed for movement of the device along the spool radial direction. Here, the axial movement platform can be used as the bottom platform for carrying the grinding detection module and deburring module. The radial movement platform is mounted on the axial platform, which is capable of following the entire device during axial movement.

For real-time grinding detection of the valve spool shoulder, an inductive single-point measuring instrument can be used, where detection is performed via a contact-type relative measurement. During these measurements, the single-point measuring instrument probe is positioned close to the end surface of the shoulder, and a preload is applied prior to grinding. In the grinding process, this preload will change with changes in the axial dimension of the end face changes. The corresponding grinding amount of the shoulder end face can be obtained from the deflection amount of the probe. Moreover, the feedback force of deburring is detected by a parallel beam force sensor mounted on the side of the

pneumatic motor. In addition, the manual fine-tuning structure of the deburring device can adjust the radial distance to an appropriate value, thereby maintaining a feedback force of ~ 1 N for the optimum deburring effect. The mechanical part of the entire device can be clamped in the slot of the S20 grinder by a wedge block, and hence, can be easily assembled and disassembled, and the parallelism requirements are satisfied. A schematic showing the design of the system is presented in Fig. 11.

After the grinding displacement of the valve spool shoulder is measured by the probe of the single-point measuring instrument, the data are transmitted to the control system in real time. The system estimates the subsequent grinding displacement by comparing the test result and the overlap amount. The data are then fed back to the micro-drive platform for driving axial movement of the valve spool until the spool is processed to a qualified position. After the grinding is completed, the pneumatic grinding pen drives high-speed rotation of the grinding head and the resulting grinding process removes the generated edge burrs. The entire system constitutes a high-precision closed-loop control system that employs the LabVIEW software for full automation of the grinding and deburring process.

3.2 Structure design of the device

The device consists of three parts, namely the supporting part, grinding detection part, and deburring part (the overall mechanical structure of the device is shown in Fig. 12). The supporting part serves as a connection to the machine tool, positioning, and bearing. The other two parts perform functions such as grinding-amount detection and deburring. A diagram showing the system structure and a picture of the actual device are shown in Fig. 12.

3.2.1 Supporting part

The supporting part can be directly suspended on the S20 precision cylindrical grinder (Fig. 13). The lower end surface of the bottom plate comes into contact with the upper end surface of the grinder guide rail and a positioning relationship is formed. The wedge block is stuck in the slot of the machine tool guide rail and is connected to the slider by screws. Furthermore, the bottom plate is fixed by pre-tightening the screws between the slider and the bottom plate. The relative radial position of the device and the machine tool is determined by the side surface beside the pre-tightening screws of the bottom plate. Therefore, this structure can be easily disassembled and assembled on demand.

3.2.2 Grinding detection part

The spool axial direction is the mounting direction of the grinding probe (which requires high precision) and, therefore, a linear motor (model AXD90S-L200-C-0.001) is used (Fig. 14). Consider the dimensions of the overall structure. To reduce the volume and weight of the entire device and meet the height requirements, the radial movement is completed by a telescopic biaxial cylinder (stroke 50 mm), and the guide rail supporting the radial movement uses a THK cross roller guide rail. The probe is composed of industrial corundum ruby, which is suitable for contact detection of the valve spool shoulder displacement. The bearing seat serves as the base carrier of the single-point measuring instrument, and is connected (via screws) to the extended end of the cylinder and the guide rail. In addition, the movement of the entire grinding-amount detection part along the spool axial direction is driven by a linear motor. Moreover, the single-point measurement instrument moves along the spool radial direction under the
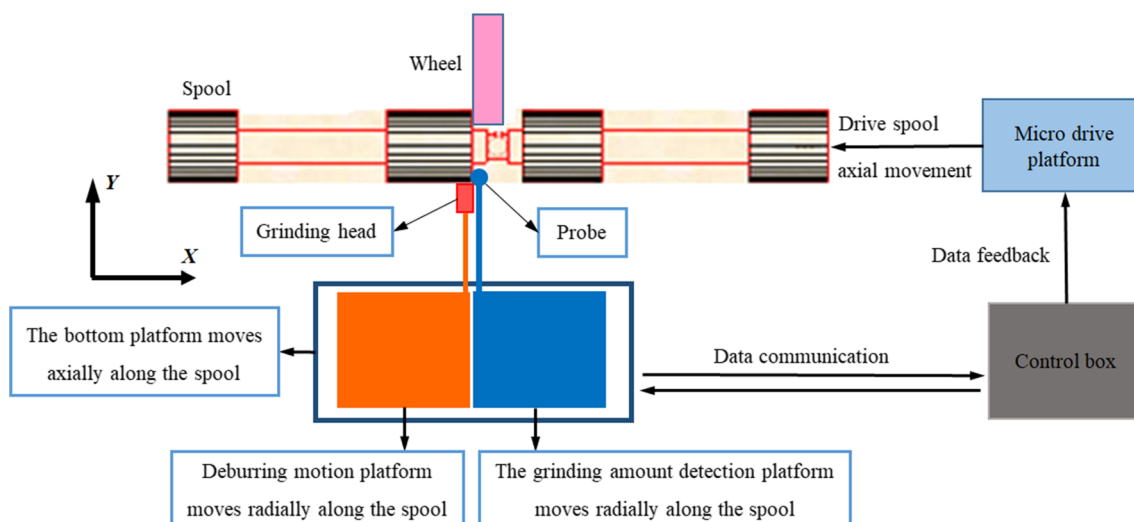

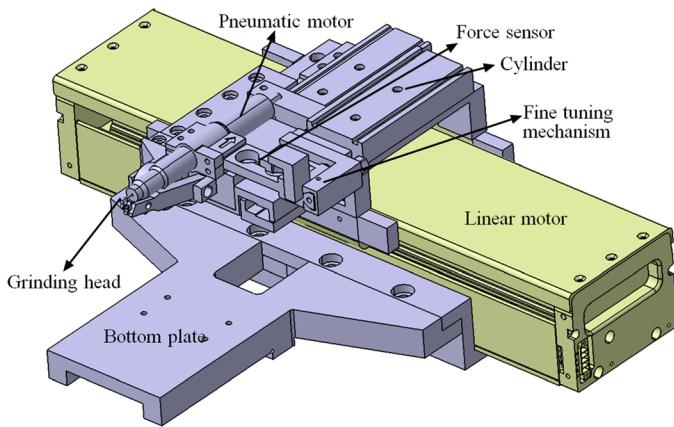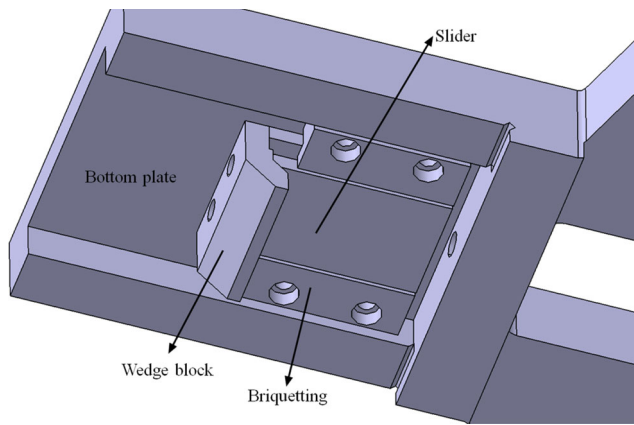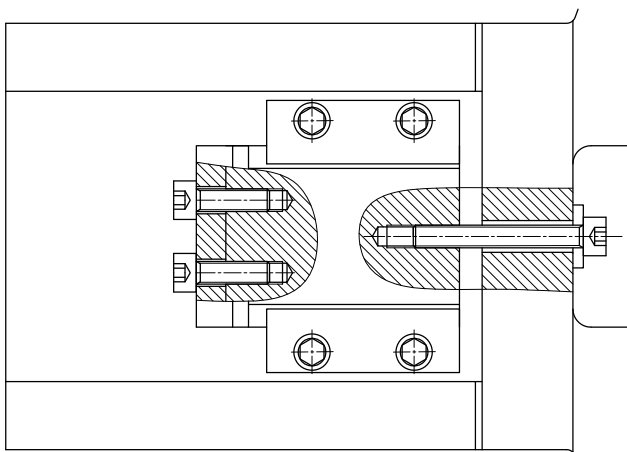**Fig. 11** System design schematic

Fig. 12 System structure design diagram and an actual device picture

action of the cylinder, thereby meeting the usage requirements.

a) Three-dimensional structure diagram

b) Two-dimensional structure diagram

Fig. 13 Structural design diagram of the supporting part. (**a**) Three-dimensional structure diagram. (**b**) Two-dimensional structure diagram

3.2.3 Deburring part

The movement mode of the deburring part is the same as that of the grinding detection part. That is, the movement along the spool axial direction and the movement along the spool radial direction is performed by a linear motor and a telescopic bi-axial cylinder, respectively. The pneumatic grinding pen drives high-speed rotation of the grinding head, thereby leading to deburring. Compared with the deburring technique performed by means of turning, no edge burr phenomena occur and the spool yield can be improved. The deburring feedback force is measured by a parallel beam force sensor (measurement range, 5 N; resolution, 1 mN), which allows fulfillment of the usage requirements. Furthermore, the distance between the shoulder edge and the grinding head differs among different types of valve spools, and hence, the radial motion position must be adjusted with a fine-tuning mechanism. A screw seat lies on the side of the force sensor (see Fig. 15) and the radial distance can be adjusted by using the screw and the screw seat (screw pitch 1 mm).

3.3 Electrical system design of the device

After the device structure design is completed, to realize the automatic processing of the valve spool shoulder, it is necessary to design the electrical part of the system and integrate the
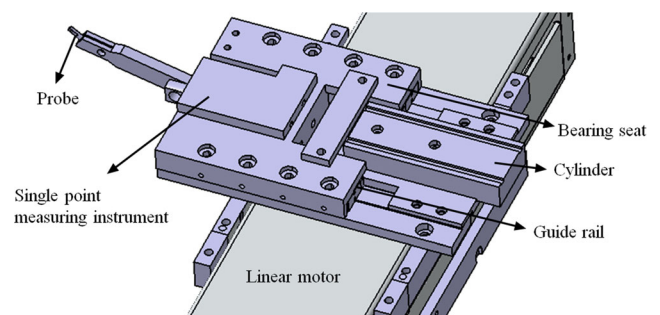

Fig. 14 Structural design diagram of the grinding detection part
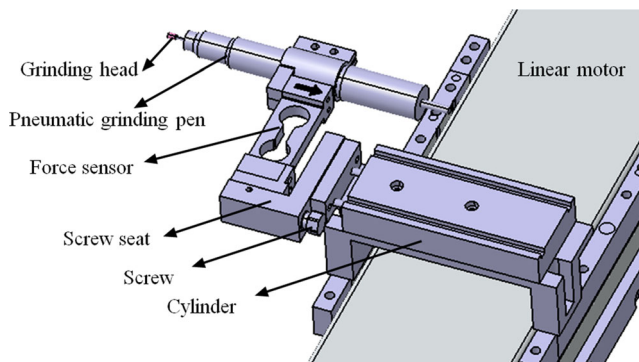
Fig. 15 Structural design diagram of the deburring part

control functions of each part, thereby allowing the control of various devices, as well as data collection and feedback. The electrical system consists of two parts, namely the pneumatic part and the electrical part.

3.3.1 Pneumatic design

The pneumatic driving part consists of a pneumatic grinding pen and two radial moving cylinders. In the structural design, the pneumatic grinding pen can withstand a rotation speed of ~65,000 rpm, which can be adjusted by the knob at the end of the pen. An inlet pressure of >0.15 MPa is required for high-speed rotational grinding. The selected pneumatic grinding pen must be connected to an air inlet, but an external connection to the top air outlet is unnecessary. However, the cylinders in the grinding-amount detection part and the deburring part undergo bidirectional movement, which requires an external air inlet and air outlet.

An electromagnetic exchange valve is needed for automatic processing of the system (see Fig. 16 for the design of the pneumatic circuit). The pressure of the air source is 0.7 MPa. If directly connected to the cylinder, this source will cause overly rapid biaxial movement of the cylinder, and shocks when the cylinder stretches out and draws back, thereby affecting the performance of the device. Therefore, a pressure-reducing valve should be

installed in front of the air inlets of the two cylinders in order to properly reduce the pressure of the air inlets. This ensures that the cylinder can slowly extend and lessen the shocks.

3.3.2 Electrical design

The electrical circuit includes a linear motor control, valve spool axial displacement drive motor control, pressure signal detection, displacement signal detection, and an electromagnetic valve. The linear motor and the micro-drive motor are controlled by their respective drivers. Furthermore, the motion control card (Altai USB1010) is connected to the driver for communication, which can output high-frequency pulses for controlling the operation of the biaxis motor.

In the deburring device, the parallel beam force sensor, SUP2, collects the grinding feedback force. The voltage amplification and A/D conversion circuit of the force sensor employ a modular digital integrated circuit. The ZL101 force measurement display is used to convert the force signal into a digital communication signal and display it, with small size and high stability.

The inner structure of the single-point measuring instrument is a solenoid differential inductance sensor. The secondary instrument circuit of this sensor requires an AC oscillation circuit for applying the generated AC sinusoidal voltage to the supply bridge of the sensor.

When the probe of the sensor is biased, the iron core inside the solenoid moves with this sensor, and an AC output signal is generated. The signal is then amplified, and subsequently processed by means of phase-sensitive detection and demodulation, thereby yielding a DC output signal. An ICL7135 A/D converter is used to convert this signal into digital quantity for output. In addition, the power supply of the circuit uses a voltage regulator, which ensures that a highly reliable output voltage is generated.

The opening and closing of the three electromagnetic valves in the pneumatic circuit must be controlled. Therefore, the four-way relay module is used to complete the on-off circuit by controlling the high and low levels. The selected USB1010 motion control card has four universal
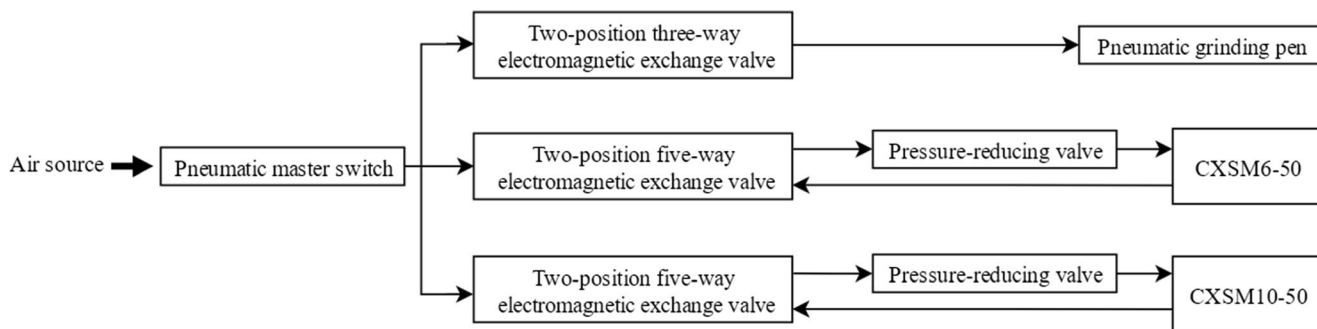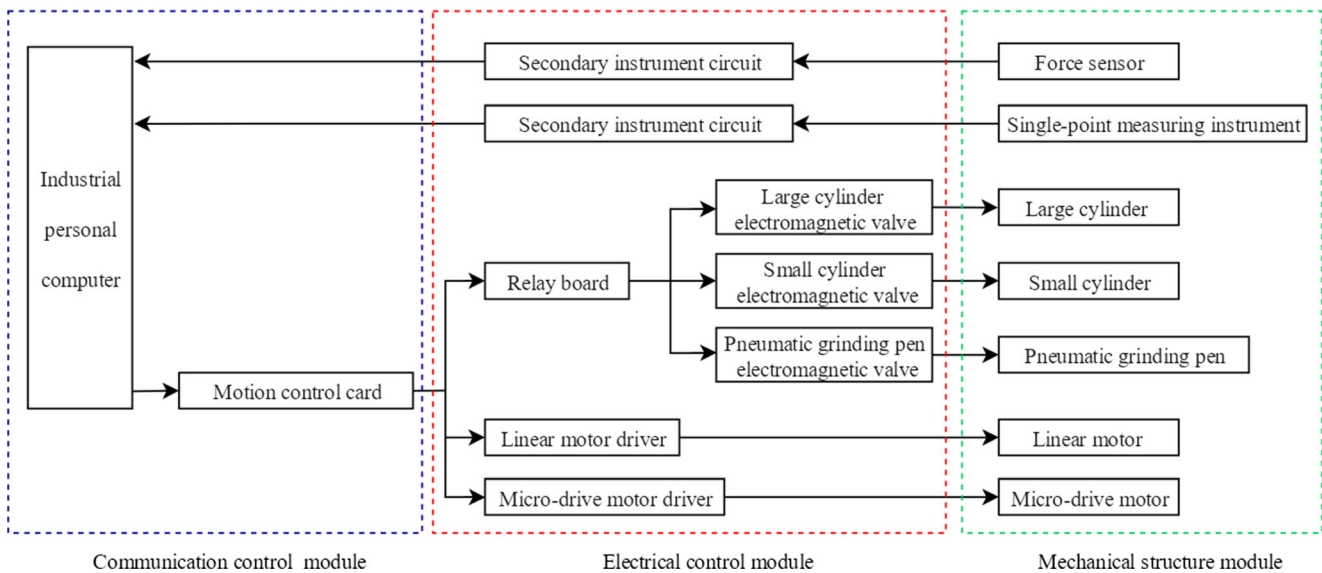

Fig. 16 Pneumatic circuit design

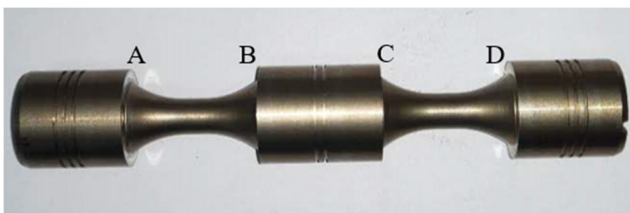**Fig. 17** Overall circuit control block diagram

input/output interfaces that can be used as the control signal output of the relay module. That is, the above circuits are integrated (see Fig. 17 for the overall circuit control block diagram).

As shown in Fig. 17, the displacement signal is collected by the single-point measuring instrument and the force sensor, processed by the secondary instrument circuit, and then input into the industrial personal computer. Subsequently, the industrial personal computer outputs the signal to the motion control card, which completes the control of the two motors and three electromagnetic valves. The industrial personal computer uses an industrial small touch control all-in-one machine, which operates rapidly and contains a total of four USB interfaces capable of meeting the communication requirements of the system.

4 Deburring test and result analysis

4.1 Spool shoulder grinding and deburring process experiment

The entire device was mounted on a S20 precision cylindrical grinder in preparation for the valve spool shoulder processing experiment (line speed of selected grinding wheel, 35 m/s;

grinding depth, 0.005 mm). Four shoulders, as shown in Fig. 18, were considered in the model. To verify the deburring effect of the device, two shoulders (A and B) were subjected only to grinding during the grinding process. The remaining two shoulders, C and D, were subjected to grinding and synchronous deburring.

After processing the valve spool shoulder, to conveniently observe the processing status of each shoulder edge, sections of the spool are obtained by cutting the valve spool along its axis using a DK77 linear cutting tool (sectional views after cutting are shown in Fig. 19). The shoulders of A, B, C, and D (Fig. 20) were observed by using a SK2008H microscope.

During the experiment, the industrial personal computer collected the grinding feedback force during the burr removal process. The time dependence of the grinding force (see Fig. 21) was then plotted from the collected data.

4.2 Result analysis

A comparison of the four groups (see Fig. 20) shows that sharp burrs formed on the shoulders of A and B, whereas the edges comprising the shoulders of C and D are relatively smooth.
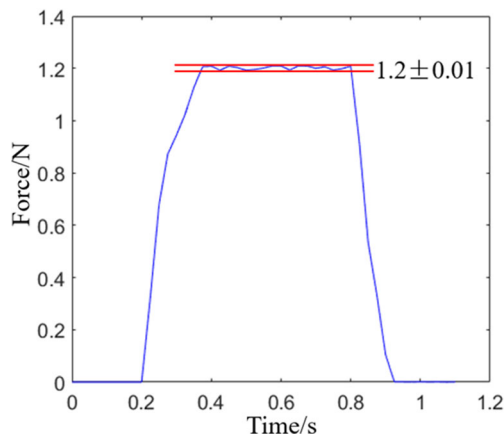

Fig. 18 Experimental spool
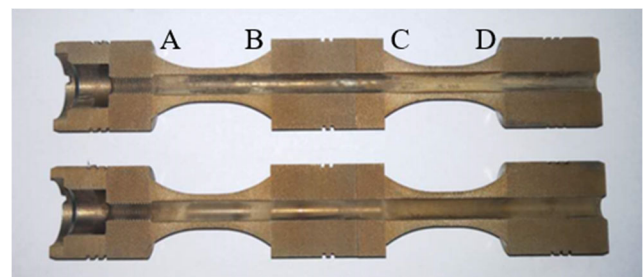
Fig. 19 Sectional drawing of the valve spool. (**a**) Shoulder A. (**b**) Shoulder B. (**c**) Shoulder C. (**d**) Shoulder D

Fig. 20 Microscopic state of each valve spool shoulder

(a) Shoulder A

(b) Shoulder B

(c) Shoulder C
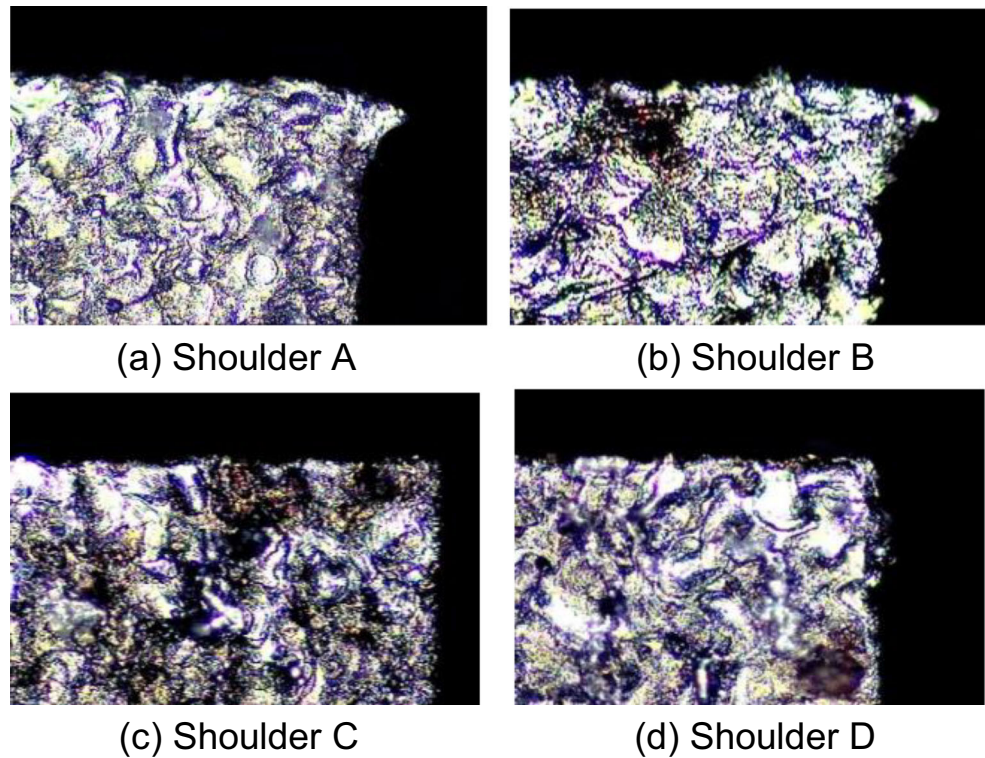
(d) Shoulder D

As shown in Fig. 20a and b, secondary burrs formed on the shoulders of A and B. Consistent with theory, the formation of edge burrs during the grinding process is induced mainly by the plastic yield flow in the negative shear direction of the cutting layer root material. The calculated burr dimensions are as follows: height, 0.012 mm; width, 0.027 mm. For the same cutting parameters, the simulated dimensions are as follows: height, 0.009 mm; width, 0.023 mm. The maximum error is 21.7%, indicating that the simulation results are credible. As shown in Fig. 20c and d, the shoulder edges of C and D are smooth, i.e., sharp burrs are absent.

Moreover, as shown in Fig. 21, during the deburring process, the grinding force varies only slightly (i.e., within ± 0.01 N). This suggests that the burr size varies slightly in the

radial range of the shoulder, and the distribution of the burrs on the edge is relatively uniform. The results also indicate that the rotating vibration of the pneumatic grinding pen has little influence on the vibration of the deburring structure. Furthermore, no resonance phenomenon is induced, consistent with the results of the modal analysis (see Fig. 10).

The analysis indicates that the designed deburring device is effective, feasible, and reliable. Compared with the traditional processing method, the device can yield significant improvement in the processing efficiency and surface quality of the valve spool.

5 Conclusions

The edge burr problem associated with the grinding process of a servo valve spool shoulder was considered in this work. To resolve this problem, a cutting model of the burrs was established and the critical conditions required for the formation of different burr types were evaluated. A single abrasive grain micro-cutting model was established and the mechanism of burr formation was analyzed. Furthermore, the main cutting parameters were determined via simulations of the deburring process. A grinding and simultaneous deburring device was designed and corresponding experiments were performed on an S20 grinder. The conclusions of the present study are summarized as follows:

Fig. 21 Time dependence of the grinding force

- The formation of primary burrs and secondary burrs is related to bending deformation and shear slip deformation. During grinding, short secondary burrs with a relatively uniform size result mainly from plastic yield flow of the cutting layer root material in the direction of negative shear.
- A single abrasive grain micro-cutting model was established, and a 128 mesh of green corundum was selected as the modeling material. The top diameter of the abrasive grain model, radius of the sphere, and cone angle are 116 μm, 9 μm, and 49.13°, respectively.
- Appropriate grinding parameters, including the grinding speed (35 m/s), grinding depth (0.005 mm), and grinding wheel particle size (128), were obtained via the single factor analysis method used for the simulations. In actual processing, the largest possible granularity values are desired.

The correctness of the single abrasive grain micro-cutting simulation was verified by means of the valve-edge edge grinding experiment. The deburring experiment was performed using the device. The results revealed that the device is effective in removing the burrs from the shoulder of the valve spool and the design of the device is feasible. Due to the burr formation mechanism and the flexibility of the burr removal device, the model established in this work is universally applicable. Moreover, the research results and conclusions can be used to guide the analysis of actual burr removal. Future work will include use of the simulation model for the prediction of grinding burrs, and the realization of burr removal and intelligent optimization.

References

1. Yang ZS, He ZB, Yang FB, Rong C, Cui XH (2018) Design and analysis of a voltage driving method for electro-hydraulic servo valve based on giant magnetostrictive actuator. Int J Appl Electrom 1:1–18
2. Li GQ, Liu W, Han WF, Guo BJ, Li YS (2018) Research on structure decoupling of passive electro-hydraulic force servo system. Adv Mech Eng 10(5):1–11
3. Zhao JB, Wang JZ, Wang SK (2013) Fractional order control to the electro-hydraulic system in insulator fatigue test device. Mechatronics 23(7):828–839
4. Hahn H, Piepenbrink A, Leimbach KD (1994) Input/output linearization control of an electro servo-hydraulic actuator. Proc IEEE Int Conf control Appl (2):995~1000
5. Wang JZ, Zhao JB, Wang SK (2014) The development and future trends of electro-hydraulic servo technology. Chinese Hydraulics & Pneumatics 5:1–12
6. Kilic E, Dolen M, Koku AB, Caliskan H, Balkan T (2012) Accurate pressure prediction of a servo-valve controlled system. Mechatronics 22(7):997–1014
7. Guo JD, Li Y, Lu HL, Qin LG, Li Y, Dong GN (2018) An effective method of edge deburring for laser surface texturing of co-Cr-Mo alloy. Int J Adv Manuf Technol 94(1–4):1491–1503
8. Pang XC, Guo H, Liu QL (2017) The design of all-in-one machine for milling groove to remove burrs. Industrial & Science Tribune 16(17):50–51
9. Chen MJ, Ni HB, Wang ZJ, Jiang Y (2012) Research on the modeling of burr formation process in micro-ball end milling operation on Ti–6Al–4V. Int J Adv Manuf Technol 62(9–12):901–912
10. Guo W, Hua M, Tse PW-T, Mok ACK (2012) Process parameters selection for laser polishing DF2 (AISI O1) by Nd:YAG pulsed laser using orthogonal design. Int J Adv Manuf Tech 59(9):1009–1023
11. Dong XB, Zhou TF, Pang SQ, Liang ZQ, Ruan BS, Zhu ZC, Wang XB (2018) Mechanism of burr accumulation and fracture pit formation in ultraprecision microgroove fly cutting of crystalline nickel phosphorus. J Micromech Microeng 28(12):1361–1389
12. Wang ZJ, Luo XY, He WT, Zhang YS (2015) Investigation into the tribological behaviors of press hardening steels on the tailored conditions. Sci China Technol Sc 58(1):97–106
13. Pratap A, Patra K, Dyakonov A.A (2019) A comprehensive review of micro-grinding: emphasis on toolings, performance analysis, modeling techniques, and future research directions. Int J Adv Manuf Technol 104:63–102
14. Niknam SA, Davoodi B, Davim JP, Songmene V (2018) Mechanical deburring and edge-finishing processes for aluminum parts—a review. Int J Adv Manuf Tech 95:1101–1125
15. Zhang DY, Zhao FF, Li Y, Li PY, Zeng QF, Dong GN (2016) Study on tribological properties of multi-layer surface texture on Babbitt alloys surface. Appl Surf Sci 390:540–549
16. Tang Q, Zhou LQ, Song WT, Li YP (2019) Finite element simulation study on the impact of single abrasive on milling burr. J Mech Sci Technol 38(10):1555–1560
17. Bandapalli C, Singh KK, Sutaria BM, Bhatt DV (2018) Experimental investigation of top burr formation in high-speed micro-end milling of titanium alloy. Mach Sci Technol 22(6):989–1011
18. Mian AJ, Driver N, Mativenga PT (2010) A comparative study of material phase effects on micro-machinability of multiphase materials. Int J Adv Manuf Technol 50(1–4):163–174
19. Dyakonov A, Gorodkova A (2018) Experimental research of cutting forces during microgrinding. MATEC Web Conf 224:1049–1053
20. Perveen A, Wong YS, Rahman M (2011) Characterisation and online monitoring of wear behaviour of on-machine fabricated PCD micro-tool while vertical micro-grinding of BK7 glass. Int J Abras Technol 4(4):304–324
21. Mathai G, Melkote S, Rosen D (2013) Material removal during abrasive impregnated brush deburring of micromilled grooves in NiTi foils. Int J Mach Tool Manu 72:37–49